ROTATION OF BALLOONS AT FLOATING ALTITUDE

TECHNICAL REPORT III

report to

OFFICE OF NAVAL RESEARCH

Arthur D. Little, Inc.

ROTATION OF BALLOONS AT FLOATING ALTITUDE

Technical Report III

Report to

OFFICE OF NAVAL RESEARCH
PHYSICS BRANCH
CONTRACT NO. Nonr 3164(00)

By

A. E. Germeles
R. M. Lucas

and

E. R. Benton
of National Center for
Atmospheric Research
Boulder, Colorado

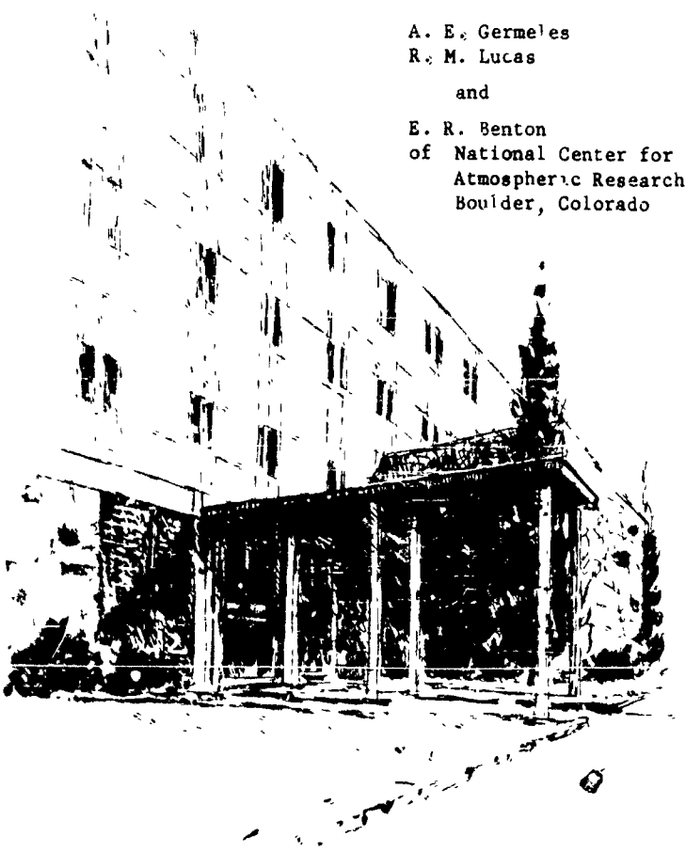

December 1963

C-62944

Arthur D. Little, Inc.

TABLE OF CONTENTS

	Page
List of Figures	v
List of Tables	vii
I. SUMMARY	1
II. INTRODUCTION	2
III. THE WAKE OF A MOVING BLUFF BODY	3
IV. DAMPING AERODYNAMIC TORQUE FOR A ROTATING SPHERE	10
A. EXPERIMENTAL SET-UP	10
B. SPHERICAL MODELS	11
C. EXPECTED FORM OF THE DAMPING TORQUE	13
D. EXPERIMENTAL RESULTS AND DISCUSSION	15
E. INTERNAL FLOW	18
V. APPARENT ADDITIONAL MOMENT OF INERTIA FOR A ROTATING SPHERE	20
A. DESCRIPTION OF THE EXPERIMENT	20
B. EXPECTED FORM OF THE APPARENT ADDITIONAL MOMENT OF INERTIA AND OTHER THEORETICAL CONSIDERATIONS	22
C. EXPERIMENTAL RESULTS AND DISCUSSION	25
VI. THE AERODYNAMIC PARAMETERS OF FULLY INFLATED BALLOONS	31
VII. DYNAMICS OF BALLOON ROTATIONS	34
A. SINUSOIDAL ANALYSIS: THEORY	35
B. SINUSOIDAL ANALYSIS: NUMERICAL EXAMPLE	36
REFERENCES	
DISTRIBUTION LIST	41

LIST OF FIGURES

Figure No.		Page
1	Formation and Shedding of Vortex Rings in the Wake of a Liquid Drop (Courtesy of "Canadian Journal of Physics")	5
2	The Wake of a Liquid Drop of Reynolds Number 360 (Courtesy of "The Physics of Fluids")	6
3	The Wake of a Liquid Drop of Reynolds Number 1040 (Courtesy of "Canadian Journal of Physics")	7
4	The Wake of a Sphere	8
5	Spherical Models Used in the Experiments	12
6	Streamlines in a Meridional Plane of (a) Rotating Disk and (b) Rotating Sphere	14
7	Damping Torque Coefficient (C_D) Versus Rotational Reynolds Number (R)	17
8	Apparatus for the Determination of the Apparent Additional Moment of Inertia	21
9	Correlation of Experimental Points (Sphere No. 2)	27
10	Correlation of Experimental Points (Sphere No. 3)	28
11	Correlation of Experimental Points (Sphere No. 5)	29

LIST OF TABLES

Table No.		Page
I	Diameters and Mass Parameters of Spherical Floats	11
II	Summary of Experimental Data	16
III	Summary of Experimental Results	26
IV	Experimental Determination of the Constant K	30
V	Values of the Aerodynamic Effects for a Balloon of 80 Feet in Radius at an Altitude of 80,000 Feet	32
VI	Amplitude of Angular Displacement in Radians for Various Values of Amplitude (T) and Frequency (ω) of Applied Torque	37
VII	Amplitude of Angular Displacement in Radians for Various Values of Amplitude (T) and Frequency (ω) of Applied Torque	38

I SUMMARY

The use of high altitude balloons as stable platforms for meteorological and astronomical observatories necessitates an investigation of the dynamic behavior of balloons. This report deals with the azimuthal rotations of the balloon-gondola system. The aerodynamic damping and inertia of the system have been mathematically formulated and experimentally verified. The forcing torque, mostly aerodynamic in nature, has been described and its order of magnitude has been estimated for known balloon rotations.

These rotations have been alleviated in the past by control systems which orient the gondola by reaction torques applied to the balloon. The aerodynamic parameters which are evaluated in this report can be useful in the design of such a control system.

II. INTRODUCTION

We believe that the principal source of the azimuthal motion are torques generated in the wake of the balloon, as noted in our Report No. 1 of this contract (Ref. 1). As the balloon moves through the atmosphere, the flow of air past the balloon separates, forming a cylindrical vortex sheet in the wake. The sheet is highly unstable and curls upon itself, thus, creating a region of highly concentrated vorticity. Eventually, this region breaks away from the sheet, and the process is repeated. The overall result is a periodic shedding of vortices in the wake. Aerodynamic torques, due to these vortices, can induce the balloon to exhibit many modes of motion. The azimuthal or rotational mode is of interest here. In order to predict the nature of these torques in quantitative terms, one must make a thorough survey of the highly complex wake.

In this report, we present a qualitative description of the wake behind a bluff body (like a sphere). Our remarks are drawn from our own experiments as well as the experiments of others.

The torque may be estimated if the motion and the dynamic parameters (inertia, damping, spring constant) of the system are known. In addition to the fabric and hardware inertia, the boundary layers contribute appreciably to the inertia of the system. The gases on either side of the balloon exert retarding torques on the balloon, the effect being that of a damping aerodynamic torque and an apparent additional moment of inertia. Experimental values of the damping aerodynamic torque on a sphere rotating with constant velocity were presented in Technical Report No. 1 (Ref. 1). Since then, we have made finer and more complete measurements, and the final results are presented in this report. Also, the experimental verification of the formula of the apparent additional moment of inertia is presented here.

With these aerodynamic parameters specified, a dynamic analysis with numerical examples is made of the coupled rotations of the full scale balloon-gondola system. The magnitude of the forcing torque is estimated for known rotations.

III. THE WAKE OF A MOVING BLUFF BODY

The flow of a viscous fluid around a bluff body can be described briefly in the following manner. Viscosity demands that the fluid touching the surface of the body be stationary with respect to the body (no-slip boundary condition). A small distance away from the surface, the flow is essentially potential (inviscid). In other words, a thin boundary layer covers the body, through which the velocity of the fluid changes very rapidly from zero at the surface to the value of the potential flow. The thickness of the boundary layer decreases with increasing Reynolds number (Re). Hence, for large values of Re, the boundary layer is thin.

The strong viscous forces in and along the boundary layer are balanced by the pressure gradient in the same direction of the potential flow outside the layer. At some point behind the front of the body, this pressure gradient may not be able to cancel the viscous forces of the boundary layer. There, the boundary layer detaches from the body. There is, now, a surface starting from the body and extending behind it in the fluid, on which the velocity of the fluid is equal to zero. In the two regions separated by this surface, the flow is in opposite directions; i.e., we have separation of the flow. The velocity gradients normal to this surface are very high. Therefore, this surface is like a vortex sheet and, being inherently unstable, curls upon itself creating a region of highly concentrated vorticity; i.e., a bound vortex. The vortex is fed from the vorticity generated at the surface of the body and, if the rate of generation of vorticity is greater than the rate of its diffusion through the fluid, the vortex grows in strength continuously. Ultimately, this bound vortex escapes and travels in the wake, and the cycle is repeated. The overall result is an occasional (often periodic) shedding of vortices in the wake. In summary, the shedding of vortices in the wake is due to the separation of the flow and the instability of the resulting vortex sheet and bound vortices.

These phenomena have been observed experimentally. For a cylinder, the shed vortices are line vortices with their axis parallel to the axis of the cylinder. They are shed in two trails. Since vortex lines must be closed (like electric current lines), the vorticity of one vortex in one trail is equal and opposite to the vorticity of one vortex in the other trail. The two vortices meet at the region of the wake corresponding to the edges of the cylinder, thus, forming a closed vorticity circuit. In the ideal case, the two trails are parallel and periodic constituting the so-called "Karman vortex street". These vortices exert forces on the cylinder, which can cause lateral motions of the cylinder as well as a rotation about its axis. Since the vorticity in one trail is equal and opposite to the vorticity in the other trail, these forces are alternating and the resulting motions oscillatory. The frequency of the oscillation is equal to the frequency of the shedding

of vortices in the wake. A curve has been obtained experimentally, and relates the dependence of the Strouhal number, St (a dimensionless parameter proportional to the frequency), on Re (see Fig. 149 of Ref. 2). Indeed, it has been shown that the frequency, in which long wires "sing" under the influence of the wind, can be predicted from this curve.

This curve shows that St increases with Re for $100 < Re < 700$, St is essentially constant for $700 < Re < 10^5$, and St increases very rapidly with Re for $10^5 < Re < 10^6$. Hence, the wake has a rather well-defined periodicity in the middle range of Re. In the last range of Re, small distrubances of the ambient flow will change the wake radically; the periodicity of the wake is lost, and the wake is very confused and turbulent.

The wake of a bluff body with a spherical shape will have the same basic features as that of a cylinder with some differences in detail due to the differences in geometry. Unfortunately, the wake of a sphere has not been studied to the same extent as the wake of a cylinder. Some revealing experimental studies have been published only recently. At the present time, it appears that there is an adequate knowledge of the wake of a sphere for Re up to about 1,000 only.

Magarvey, et al., (Refs. 3, 4 and 5) have taken some excellent photographs of the wake of a colored liquid drop falling freely in water. Initially, the drop was accelerating, but it reached a constant velocity ultimately. Figure 1 shows the formation of the wake. As the drop was accelerating, the flow began to separate and a cylindrical vortex sheet appeared (a). This sheet, being inherently unstable, curled upon itself more and more (b and c) forming a bound vortex ring. As the vorticity of the vortex ring increased, it began to break off from the drop. This is shown in photograph (d) taken 0.01 second before the first vortex ring was discharged in the wake. Note that the ring is discharged at a distance behind the drop of the order of magnitude of the diameter of the drop. Figure 2 shows the wake of a drop falling with constant velocity corresponding to Re = 360 ((b) is 10 seconds later than (a) and shows the diffusion of the vortex elements). The vortex elements are distorted rings interconnected with line vortices. There is a definite periodicity and a separation of the vortices in two trails. The vorticity of the rings in both trails is in the same direction.

Magarvey obtained an experimental curve for the dependence of St on Re for $270 < Re < 390$. As Re was increased further, the wake began to lose its periodicity. This is shown in Figure 3 for Re = 1040

Figure 4 shows representative results from our own rough experiments. A ping-pong ball was placed in a uniform stream, whose speed was varied so that values of Re up to 6,000 were obtained. Ink, flowing out from small holes on the equator of the ball, made the wake visible. At Re = 600 (Fig. 4a), the wake was similar to that obtained by Magarvey,

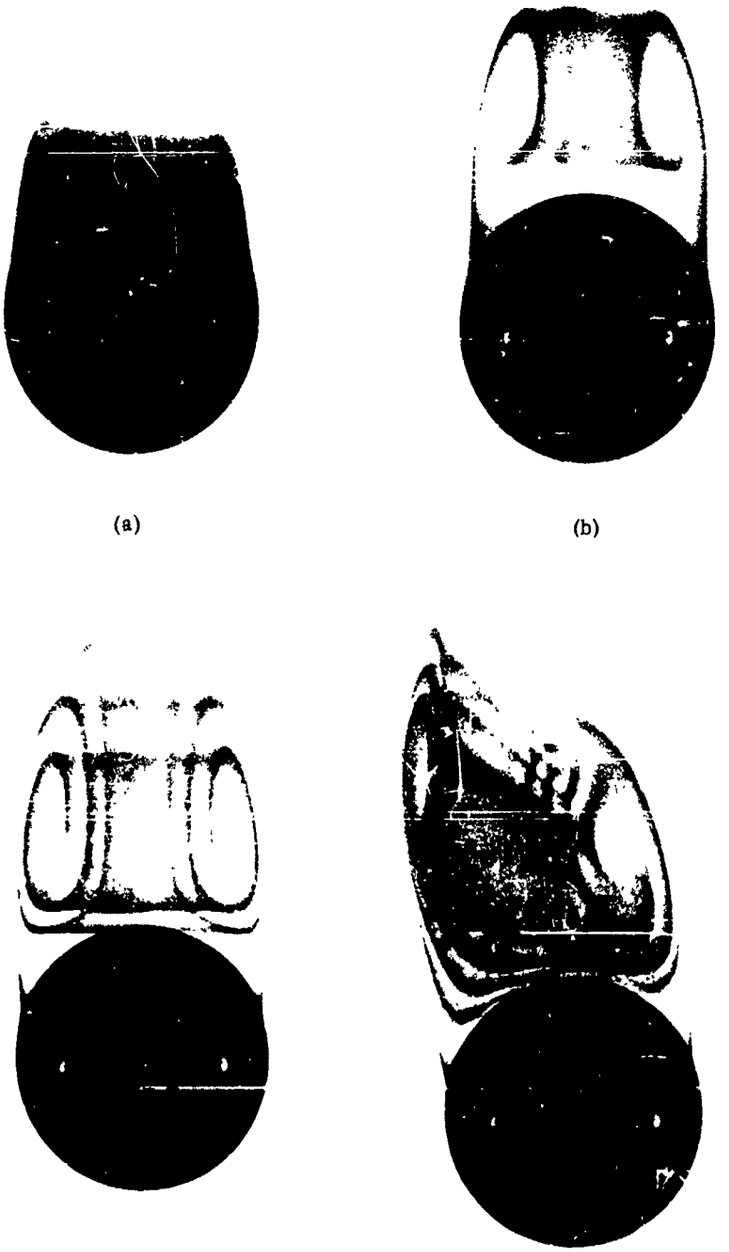

FIGURE 1 FORMATION AND SHEDDING OF VORTEX RINGS IN THE WAKE OF A LIQUID DROP (COURTESY OF THE "CANADIAN JOURNAL OF PHYSICS")

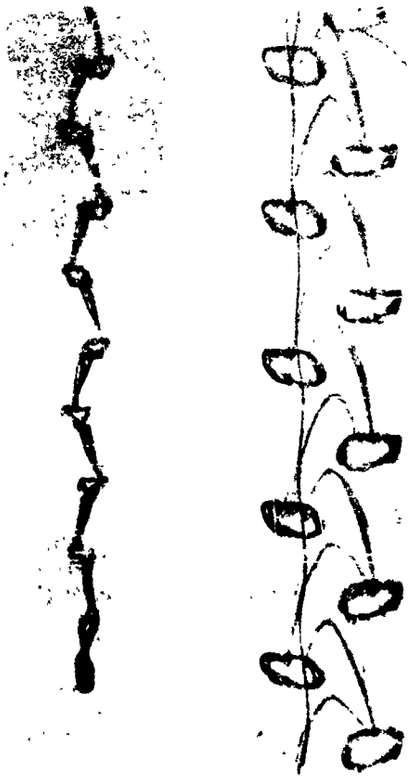

(a) (b)

FIGURE 2 THE WAKE OF A LIQUID DROP OF REYNOLDS NUMBER 360. (COURTESY OF "THE PHYSICS OF FLUIDS")

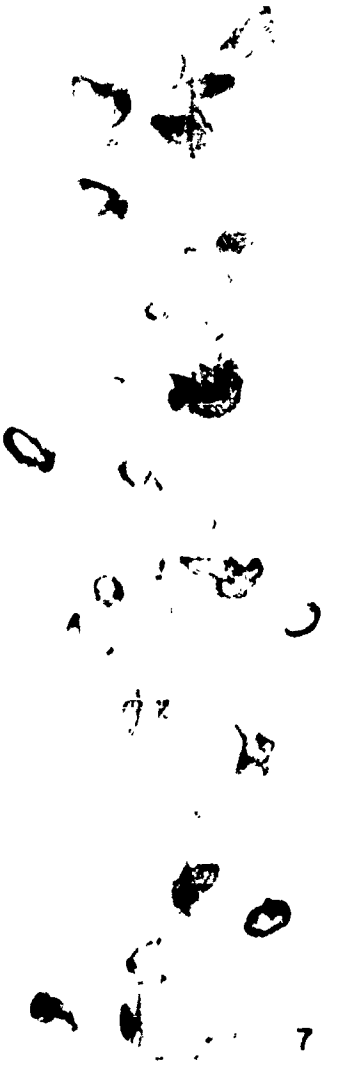

FIGURE 3 THE WAKE OF A LIQUID DROP OF REYNOLDS NUMBER 1040 (COURTESY OF "CANADIAN JOURNAL OF PHYSICS")

(a) Re = 600

(b) Re = 1, 200

(c) Re = 2, 400

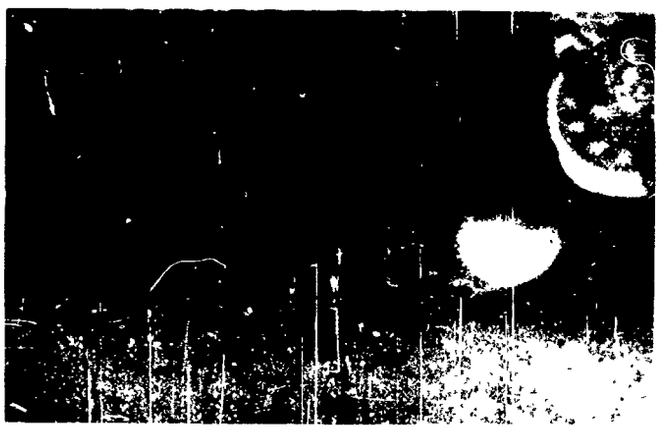

(d) Re = 4, 800

FIGURE 4 THE WAKE OF A SPHERE

and it had a definite periodicity. At Re = 1200 (Fig. 4b), some periodicity was still visible. At Re = 2400 (Fig. 4c), the wake was quite confused with some regions of concentrated vorticity. At Re = 4800 (Fig. 4d), the wake was almost uniformly turbulent and all periodicity disappeared.

This apparent disorder in the wake of a sphere at values of Re above 1,000 must be due to the presence of a high degree of ambient turbulence, or a very sensitive dependence of St on Re, or both. Accurate and well-controlled experiments will clear up this point. At the present time one thing is rather clear; i.e., for Re in the range of about one to a few thousands, the wake of the sphere is incipiently unstable, and very small disturbances of the uniform stream (like inherent turbulence, small ambient flow disturbances, etc.) can alter the form of the wake and destroy its periodicity. This has been confirmed by other investigators (verbal communications).

As in the case of the cylinder, the wake of the sphere exerts forces and torques on the sphere. Therefore, if the sphere is free, it can assume quite a few modes of lateral motion and rotation. The same phenomena will occur for a body like a balloon. These facts have been confirmed by our experiments with balls and scaled balloons falling freely in a water tank (Ref. 1).

IV. DAMPING AERODYNAMIC TORQUE FOR A ROTATING SPHERE

Since the azimuthal rotation of balloons is especially crucial while they are at or near their floating altitude, we have restricted our attention to the case of fully inflated balloons. A balloon at floating altitude is idealized as a spherical shell with an extremely small thickness to radius ratio. The spherical shape is believed to be close enough to the onion-shape of actual balloons to make the results applicable, while preserving geometric simplicity for ease of analysis. It is further assumed that damping is independent of the small values of vertical velocity.

A simple experiment (Ref. 1, p. 36) was previously described for obtaining the torque required to overcome viscous skin friction on a steadily rotating sphere. The goal of this experiment was to provide a basis for estimating the damping aerodynamic torque which opposes the rotations of rising and falling balloons.

The results of the first experiment were sufficiently encouraging to warrant refining the experiment. While no better means of measuring small steady torques was found, more precise measurements have been carried out on a greater number of models which were more highly spherical. The data extend over a wider range of variables and are more reliable than the previous data.

A. EXPERIMENTAL SET-UP

A stainless steel cylindrical tank--3 feet in diameter, 2.5 feet deep--was filled with water. Brookfield viscometers (Model RVF) were used to spin the models at constant speed about a vertical axis and to indicate the torque required to maintain the steady rotation. One viscometer had operating speeds of 100, 50, 20, and 10 rpm; the other, 20, 10, 4, and 2 rpm. Each in turn was carefully mounted with its shaft at the center of the tank. The models were completely filled with water and submerged so that the "north pole" was about 3 inches beneath the free surface.

Eccentricity was minimized by very careful mounting. Still a small AC disturbance, due to eccentricity, appeared in some viscometer readings. The average readings over a cycle should not be affected by it.

Sufficient time was allowed after starting the synchronous motor in the viscometer for the starting transients to damp out (see further discussion below).

B. SPHERICAL MODELS

The models were spherical aluminum floats (Fig. 5). Each float consisted of two hemispheres, of about 0.025 inch wall thickness, welded together at the equator. The welded seams were filed down flush, and each sphere was sprayed with clear lacquer.

The nominal diameters were 2, 3, 4, 5, 6, 7, and 8 inches, but the two largest spheres could not be used. They put enough weight on the viscometer bearing to increase bearing drag prohibitively. The actual equatorial diameters as measured and the mass parameters (for future reference) are tabulated in Table I. Generally, the equatorial and polar diameters agreed within about 1/64 inch, but the polar diameter of Sphere Number 5 was about 3/64 inch less than its average equatorial diameter.

TABLE I

DIAMETERS AND MASS PARAMETERS OF SPHERICAL FLOATS*

Sphere No.	Diameter (CM)	Mass (GM)	Moment of Inertia ($GMCM^2$)**
1	5.02	19.5	81.9
2	7.58	67.3	646
3	10.12	128.0	2,190
4	12.66	197.6	5,290
5	15.16	186.5	7,170
6	17.66	399.7	20,800
7	20.20	478.1	32,500

*Obtained from the Chicago Float Works, 2330 South Western Avenue, Chicago 8, Illinois.

**Computed from Moment of Inertia = 1/6 (Mass)(Diameter)^2.

FIGURE 5 SPHERICAL MODELS USED IN THE EXPERIMENTS

C. EXPECTED FORM OF THE DAMPING TORQUE

In Technical Report No. 1 (Ref. 1) the form of the aerodynamic damping torque on a rotating sphere was deduced from theoretical considerations of the boundary layer near a flat plate moving with constant velocity. Here, the form of the torque will be derived from the flow of a rotating disk, which has many similarities with the flow of a rotating sphere and has been completely solved.

Figure 6 shows the streamlines of the flow in a meridional plane of an infinite disk and a sphere of radius a, both rotating with a constant angular velocity ω. Except in the neighborhood of the equator, the flow of the sphere is quite similar to the flow of the disk. Throughout the disk the boundary layer thickness is constant. For the sphere, the two boundary layers, which start from the poles, grow towards the equator, where they collide and erupt. (Nor is the flow of the rotating sphere near the equator like the flow of a rotating cylinder, since in the latter there is no secondary outflow at all.)

For the disk, the angular velocity of the fluid decreases to about 0.03ω in a distance δ away from the disk, which is given by (see Ref. 2, Section 43):

$$\delta = 4.5\sqrt{\frac{\mu}{\rho\omega}} \tag{1}$$

where μ and ρ are the viscosity and density of the fluid, respectively. Taking δ as the boundary layer thickness for the sphere and using the local velocity $v = \omega a \sin\theta$, we find that the shearing stress $(\pi \mu v/\delta)$ acting on the sphere at θ is approximately equal to $0.222\ (\rho\mu)^{1/2}\omega^{3/2}$ $a\sin\theta$. Then the damping torque, D, which is equal to the summation over the sphere of the product of the shearing stress by the area by the distance from the axis, is approximately given by:

$$D \cong \int_0^{\pi} \left[0.222\ (\rho\mu)^{1/2}\ \omega^{3/2}\ a \sin\theta\right](2\pi a^2 \sin\theta\, d\theta)(a \sin\theta).$$

Therefore,

$$D \cong 1.9\ (\rho\mu)^{1/2}\ \omega^{3/2}\ a^4. \tag{2}$$

Let us define the pertinent Reynold's number, R, by:

$$R = \frac{\rho\omega a^2}{\mu} \tag{3}$$

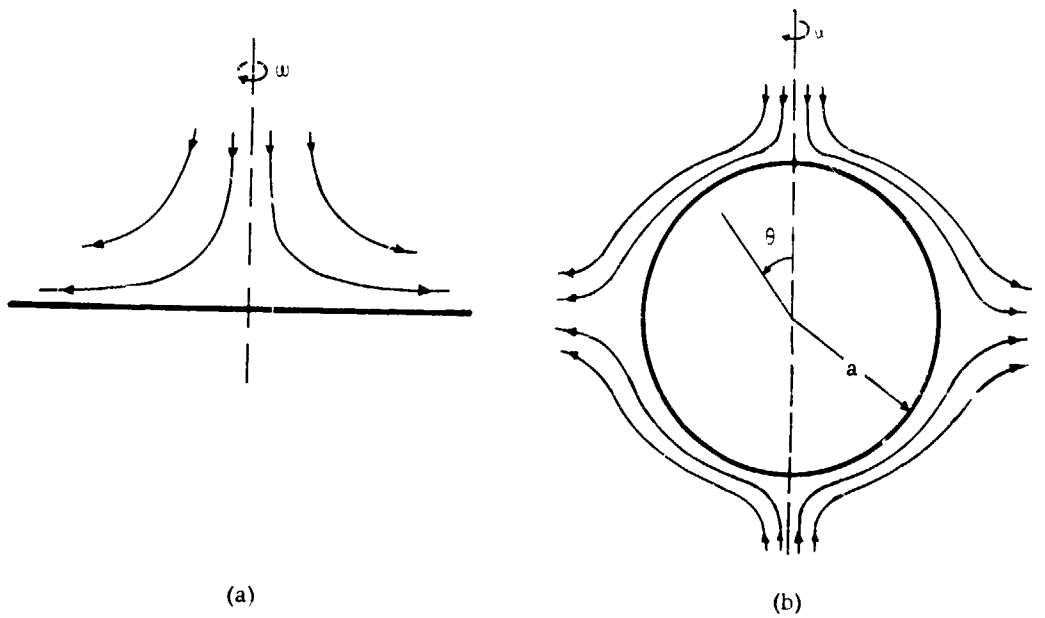

FIGURE 6 STREAMLINES IN A MERIDIONAL PLANE OF (a) ROTATING DISK AND (b) ROTATING SPHERE

and a dimensionless drag coefficient, C_D, by:

$$D = \rho \omega^2 a^4 C_D \tag{4}$$

Then Equation 2 can be put in the form:

$$C_D \cong 1.9 R^{-1/2} \tag{5}$$

The form of Equations 2 and 5 will be the guide in correlating the experimental results.

D. EXPERIMENTAL RESULTS AND DISCUSSION

The experimental data are tabulated in Table II. Each datum point tabulated is the average of at least three tests. The repeatibility of the torque measurements was about $\pm$ 3.6 dyne-cm.

Figure 7 shows the experimental data plotted non-dimensionally as C_D versus R. In the experiments R was varied from 670 to 27,300; the torque varied from 10 dyne-cm to 7130 dyne-cm (i.e., by an amount approaching three orders of magnitude). Over this wide range, the data are very well described by the following simple law:

$$C_D = 3.6 R^{-1/2} \tag{6}$$

which appears as the solid line in Figure 7. Combined with Equation 4, this leads to the formula for the data:

$$D = 3.6 (\rho \mu)^{1/2} a^4 \omega^{3/2} \tag{7}$$

This compares well with the scanty previous data summarized by Equation 4.3 of Reference 1 (p. 38). As the spheres were filled with water, Equation 7 represents the total torque from external and internal flows.

Equation 6 shows that C_D is a function of the Reynold's number only. This is expected since the drag here is entirely viscous. The nonlinear dependence of the torque on ω (D proportional to $\omega^{3/2}$ instead

TABLE II

SUMMARY OF EXPERIMENTAL DATA

Sphere No.	ω rad/sec	Torque, D, dyne-cm	$\frac{D}{(\rho\mu)^{1/2}\omega^{3/2}a^4}$	$C_D = \frac{D}{\rho\omega^2 a^5}$	$R = \frac{\rho\omega a^2}{\mu}$
1	10.48	471	3.54	0.0431	$6.71\cdot10^3$
	5.24	162	3.44	0.0593	$3.36\cdot10^3$
	2.096	37.7	3.16	0.0864	$1.34\cdot10^3$
	1.048	10.06	2.38	0.0919	$6.71\cdot10^2$
2	10.48	2440	3.52	0.0284	$1.54\cdot10^4$
	5.24	877	3.58	0.0409	$7.68\cdot10^3$
	2.096	220	3.55	0.0640	$3.08\cdot10^3$
	1.048	73.6	3.36	0.0857	$1.54\cdot10^3$
3	10.48	7130	3.23	0.0196	$2.73\cdot10^4$
	5.24	2945	3.78	0.0324	$1.37\cdot10^4$
	2.096	733	3.72	0.0504	$5.46\cdot10^3$
	1.048	253.5	3.63	0.0695	$2.73\cdot10^3$
4	2.096	1746	3.62	0.0392	$8.55\cdot10^3$
	1.048	675	3.96	0.0606	$4.27\cdot10^3$
	5.24	6150	3.43	0.0222	$2.40\cdot10^4$*
	2.096	1680	3.70	0.0379	$9.56\cdot10^3$*
	1.048	589	3.67	0.0531	$4.78\cdot10^3$*
5	2.096	3650	3.91	0.0334	$1.37\cdot10^4$*
	1.048	1210	3.67	0.0443	$6.86\cdot10^3$*
	0.4192	331	3.97	0.0758	$2.74\cdot10^3$*
	2.096	4020	4.07	0.0367	$1.23\cdot10^4$
	1.048	1393	3.98	0.0508	$6.13\cdot10^3$
	0.4192	392	4.43	0.0895	$2.45\cdot10^3$

* For entries with and without asterisk, the water temperature was 26°C and 21°C, respectively. The resulting change in viscosity caused slightly different values of R for the same values of a and ω.

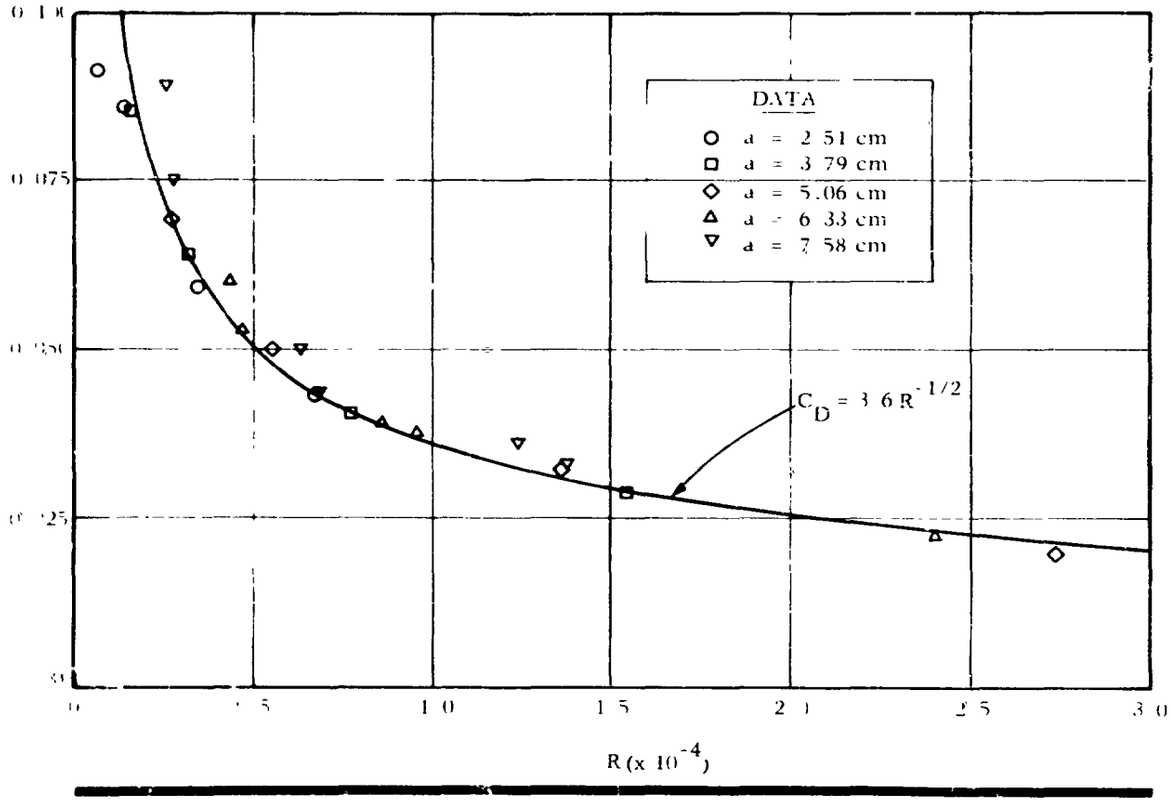

FIGURE 7 DAMPING TORQUE COEFFICIENT (C_D) VERSUS ROTATIONAL REYNOLDS NUMBER (R)

of ω as, for instance, in the case of a rotating cylinder) is, of course, due to the existence of a boundary layer whose thickness is proportional to $\omega^{-1/2}$ (see Section IV-C).

Thus, it has been verified that the dependence of D on the various parameters of the problem is of the form anticipated from theoretical considerations in Section IV-C. The constant of proportionality has been determined, and it is essentially independent of the Reynold's number for the wide range of Reynold's numbers considered here (from 670 to 27,300). Considering the fact that both the internal and the external flows have contributed equally to the torque given by Equation 7 (see Section IV-E), it is seen that there is a satisfactory agreement between theory and experiment even in the numerical value of the constant of proportionality (1.9 by theory and 3.6/2 = 1.8 by experiment). But this should rather be considered as a coincidence, since in the theory the value of this constant depends on what exactly is taken as the thickness of the boundary layer. In Section IV-C we defined the thickness of the boundary layer as being equal to the distance from the disk at which the angular velocity of the fluid decreases to 0.03ω. We can define this thickness at a different velocity decrease (say 0.1ω or 0.01ω), and the value of the constant in Equation 2 will be different but the form of this equation will be the same. All that the present theory is expected to give is the correct order of magnitude for the constant of proportionality.

E. INTERNAL FLOW

As mentioned at the beginning of Section IV-A, the models were completely filled with water. Therefore, there was an internal as well as an external flow. The two flows can differ greatly in the following respect. In the outer flow, the effects of viscosity continuously diffuse outward so that the fluid is always sheared at the surface. However, inside the sphere, the effects of viscosity accumulate, and if the steady sphere rotation persists long enough, then the fluid inside may rotate with the sphere as a rigid body. When this happens, there is no shearing at the inner surface of the sphere and, therefore, no torque acting on it.

The effects of viscosity diffuse inward to a depth equal to the radius a in a time τ of the order $\rho a^2/\mu$. It will be at least of this order of time before rigid body rotation of the internal fluid is possible. For the smallest sphere used in the experiments, τ is of the order of 11 minutes. All readings were taken in much shorter times after starting the rotation, so we infer that the internal boundary layer was relatively thin and the data contain contributions from internal and external flows.

In order to apply the present results to balloons, which have different fluids inside and outside, it is necessary to determine the relative contributions of internal and external flows to the total torque. An attempt to perform this separation of effects experimentally was not successful. The models were first filled with water and rotated in air; then filled with air and rotated in water. In both cases, there was too much vertical load on the viscometer bearing to yield any results of value. This difficulty could probably be avoided in the future by using alcohol and water for the two working fluids, and this experiment is contemplated.

On the other hand, since in the experiment both internal and external boundary layers were very thin, it seems reasonable to assume that the internal and external flows contributed the same amount to the total measured torque. This assumption is supported by the results of Lamb (Ref. 6), who analyzed theoretically the small amplitude rotational oscillations of spherical shells with fluid either inside or outside the shell. He found that the hydrodynamic torques from internal and external flows are identical when the boundary layers are very thin.

V. APPARENT ADDITIONAL MOMENT OF INERTIA FOR A ROTATING SPHERE

The preceding section has dealt with the torque arising from the steady rotation of the zero position. However, an additional reactive torque is associated with rotational accelerations, which is the subject of this section.

When any solid body moves with constant velocity in an incompressible and inviscid fluid, the net force exerted by the fluid on the body is equal to zero. On the other hand, when the body moves with a constant acceleration, the surrounding fluid exerts on the body a net retarding force which is proportional to the acceleration. This effect has become known as the "apparent or induced mass" effect, since the body appears to have more mass when accelerated in the fluid.

For a smooth sphere accelerating angularly about its axis in a viscous fluid, a similar type of effect occurs. However, the physical mechanism causing this effect is now different. Here, viscosity demands a "no-slip" boundary condition on the surface of the sphere (or balloon). Consequently, whenever the balloon accelerates angularly, some of the surrounding air and contained helium must accelerate with the balloon. Hence, a net retarding torque is exerted on the balloon by the air and helium. In addition to a damping effect, this torque contains an inertial effect referred to as the "apparent additional moment of inertia" of the balloon.

For most solid bodies, with thin boundary layers, this increase in inertia is negligible compared to that already in the system by virtue of solid mass. However, fully inflated balloons have a very small moment of inertia (for bodies of their size), and the apparent additional moment of inertia is significant. The following experiment was intended to provide an estimate of the effect.

A. DESCRIPTION OF THE EXPERIMENT

In the experiment, a sphere, immersed in water, was given a constant initial rotation and then the decay of the rotation, due to the viscosity of water, was recorded. From this record, the apparent additional moment of inertia of the sphere was calculated.

A photograph of the experimental set-up is shown in Figure 8. A tank, 3 feet in diameter, was filled with clean tap water to a level of 2.5 feet. Some of the spherical models, described in Section IV-B, were threaded on the end of a 12-inch long and 1/4-inch diameter precision ground stainless steel shaft. The shaft was placed in a 4-inch long stainless steel cylindrical bearing holder having two precision stainless steel bearings, one at each end. This system was suspended

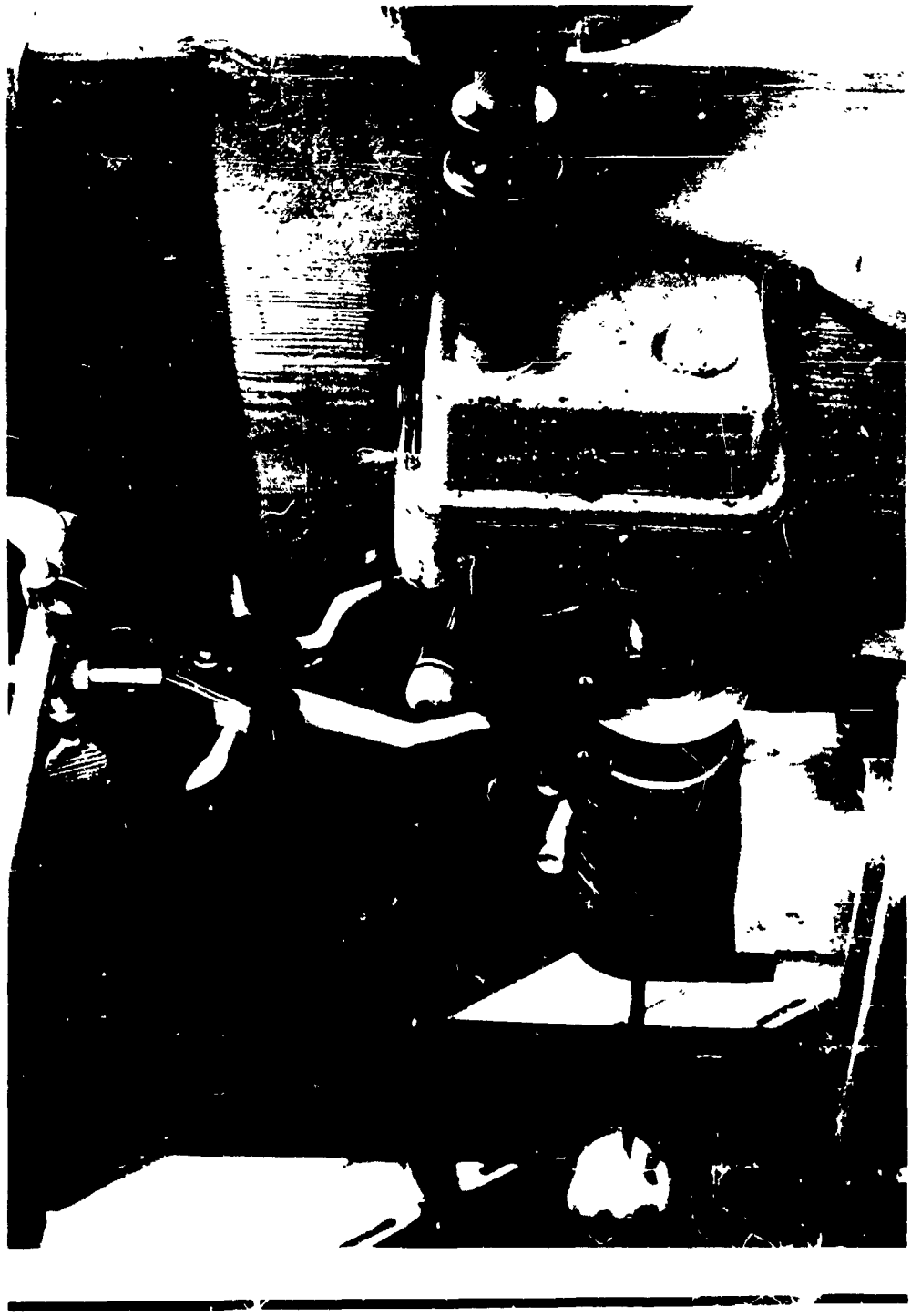

FIGURE 8 APPARATUS FOR THE DETERMINATION OF THE APPARENT ADDITIONAL MOMENT OF INERTIA

vertically along the centerline of the water tank by mounting the bearing holder to a heavy wood framework (see photograph). The upper bearing was a thrust bearing supporting the net weight of the model and shaft, while the lower was a simple radial bearing to minimize lateral motions. From the manufacturer's data, the frictional torque of the bearing is about 200 cm dynes for a thrust of 200 gm. The level of the water in the tank was about 5 inches above the top of the model.

The upper end of the shaft protruded upwards from the bearing holder about 2 inches. There, a thin aluminum circular disk (to be described later) was attached to the shaft in a horizontal position and, above the disk, a tee-shaped driving yoke. Located above the yoke was a driving mechanism consisting of a laboratory stirrer with variable speed coupled to a "Zero-Max" speed reducer. The output of the driving mechanism was variable from zero to about three revolutions per second. On the output of the speed reducer, there was a simple two-pin clutch which engaged the tee-shaped driving yoke. After the system was brought up to a preselected speed, the clutch was disengaged and the rotating mass was free to slow down. The decay of the rotation of the spherical model, due mostly to viscous effects, was recorded by an optical system.

The light source (prefocused beam) and the detector (photo-duo-diode) of the optical system are mounted opposite to each other in a C-shaped frame. In the experiment, this frame was placed so that the aluminum disk interrupted the light path. The disk had small holes, placed evenly on a circumference, through which the light beam passed as the disk rotated. Thus, a pulsed signal was generated by the detector, which was amplified and displayed by a time-base event recorder. The resulting data, consisting of a sequence of sharp pulses, gave the angle of rotation versus time. From these, the angular velocity of rotation was calculated as a function of time.

Wobble, due to eccentricity, was minimized by very careful mounting and by inserting soft rubber in the mounting of the bearing holder to the wood framework. To reduce bearing loads, the models were filled with water. All experiments were performed in calm water.

The initial speeds were selected so that, for the most part of the duration of the decay, the Reynold's number was within the range in which the damping aerodynamic torque was measured in Section IV (700 to 27,000).

B. EXPECTED FORM OF THE APPARENT ADDITIONAL MOMENT OF INERTIA AND OTHER THEORETICAL CONSIDERATIONS

Consider the sphere rotating with a constant angular velocity ω. It has been pointed out in Section IV-C that the flow is of the same similar to that of a rotating disk (see Fig. 6). Taking the thickness

of the boundary layer δ as given by Equation 1, the total angular momentum of the fluid in the boundary layer of the sphere is given approximately by:

$$\int_0^{\pi} (\rho)\left(\frac{\omega\delta}{2}\right)(a^2 \sin^2\theta)(2\pi a^2 \sin\theta \, d\theta) = 19\,(\rho\mu)^{1/2}\,\omega^{1/2}\,a^4$$

The torque exerted by the fluid on the sphere is the steady torque D dealt with in the preceding section.

Suppose, now, that the angular velocity of the sphere is changed by an amount $\Delta\omega$ in a time Δt. The surrounding viscous fluid will resist this change, and in addition to the steady torque D, it will exert on the sphere a torque equal to the time rate of change of its angular momentum as found above. Therefore, the apparent additional moment of inertia I_A of the sphere is given approximately by:

$$I_A \cong 19\,(\rho\mu)^{1/2}\,\omega^{-1/2}\,a^4 \qquad (8)$$

Actually, this is a quasi-steady state analysis, not always valid. It has been assumed that the time Δt, in which the change $\Delta\omega$ occurs, is much larger than the time required for a disturbance occurring at the surface of the sphere to diffuse through the boundary layer, so that the boundary layer remains just about fully grown during the change in ω. This latter time is of order $\rho\delta^2/\mu = 1/\omega$. The condition for the validity of the above analysis is a condition on the magnitude of the angular acceleration of the sphere, which can be stated as:

$$\frac{\Delta\omega}{\Delta t} << \omega^2 \qquad (9)$$

Neglecting bearing friction, the rotation of the sphere must satisfy the following differential equation:

$$\frac{d}{dt}\left[(I + 2I_A)\,\omega\right] + 2D = 0 \qquad (10)$$

where I is the material moment of inertia of the spherical shell. The factor of 2 appearing in front of I_A and D accounts for both external and internal flows, which, it is assumed, contribute equally (see Section Iv-E). I_A will be taken in the form of Equation 8 but with an unknown constant of proportionality to be determined from the experiment. D will be taken as found in Section IV. That is:

$$I_A = K (\rho\mu)^{1/2} a^4 \omega^{-1/2} \tag{11}$$

$$D = 1.8 (\rho\mu)^{1/2} a^4 \omega^{3/2} \tag{12}$$

Let ω_o denote the value of ω at t = 0. Substituting Equations 11 and 12 in Equation 10 and introducing the following dimensionless quantities:

$$\tau = \frac{3.6 (\rho\mu)^{1/2} a^4 \omega_o^{1/2}}{I} t \tag{13}$$

$$\alpha = \frac{(\omega_o)^{1/2} I}{K (\rho\mu)^{1/2} a^4} \tag{14}$$

the solution of Equation 10 is:

$$\left(\frac{\omega_o}{\omega}\right)^{1/2} = -\alpha + \left[(1 + \alpha)^2 + \alpha \tau\right]^{1/2} \tag{15}$$

Notice that the parameter α is the ratio of the material moment of inertia of the spherical shell to the apparent additional moment of inertia due to the external or internal flow at initial conditions. τ is a dimensionless time. The experimental results will be plotted as $(\omega_o/\omega)^{1/2}$ versus τ. Then from the family of curves given by Equation 15, the curve that fits the experimental results best will be selected. This determines the value of α from which the unknown constant K can be computed.

C. EXPERIMENTAL RESULTS AND DISCUSSION

The results of three experimental runs are tabulated in Table III. The three models were filled with water. The results satisfy the following three conditions, and therefore, the theory developed in the preceding section is applicable:

1. The total time for each run is much less than $\rho a^2/\mu$ and, therefore, the assumption, that the hydrodynamic effects of the internal and external flows are equal, seems reasonable.

2. The Reynold's number ($\rho \omega^2 a/\mu$) is within the range (700 to 27,000) in which the damping aerodynamic torque has been determined.

3. The condition of small angular accelerations, as stated by Expression 9, is satisfied.

The experimental points are shown in the normalized form $[(\omega_o/\omega)^{1/2}$ versus $\tau]$ on Figures 9 - 11. Notice that there is an oscillation due to a slight wobble of the models. Three theoretical curves (Equation 15) are drawn for each experimental run. In each case, the middle curve represents the best value of the parameter α. The value of α for each run, as well as the corresponding value of the unknown constant K (computed from Equation 14), is shown in Table IV. The average value of K for the three runs is .22. Therefore, for either external or internal flow:

$$I_A = 22 (\rho\mu)^{1/2} a^4 \omega^{-1/2} \qquad (16)$$

Notice that the theoretical and experimental values of the constant of proportionality in the formula of I_A (Equations 8 and 16) agree quite well (see, also, the last paragraph of Section IV-D).

We believe that there is enough evidence, in the above experimental results, supporting our contention that Equation 16 will give, at least, a fair estimate of I_A for the internal and external flows under the above stated three conditions.

TABLE III

SUMMARY OF EXPERIMENTAL RESULTS

Sphere #2				Sphere #3				Sphere #5			
Time (sec)	Angular Velocity ω (rps)	Normalized Time τ	$(\omega_o/\omega)^{1/2}$	Time (sec)	Angular Velocity ω (rps)	Normalized Time τ	$(\omega_o/\omega)^{1/2}$	Time (sec)	Angular Velocity ω (rps)	Normalized Time τ	$(\omega_o/\omega)^{1/2}$
0	2.000	0	1.00	0	1.000	0	1.00	0	0.2366	0	1
0.50	1.722	0.21	1.08	0.73	0.833	0.20	1.10	1.95	0.1826	0.40	1.14
1.34	1.290	0.55	1.25	2.14	0.538	0.59	1.36	4.42	0.1449	0.91	1.28
2.19	1.081	0.91	1.36	5.85	0.346	1.60	1.70	7.55	0.1146	1.55	1.44
2.69	0.930	1.11	1.47	10.90	0.231	2.99	2.08	11.40	0.0952	2.34	1.58
3.37	0.776	1.40	1.61	15.08	0.186	4.14	2.32	16.09	0.0756	3.31	1.77
4.80	0.633	1.99	1.82	19.63	0.148	5.39	2.60	22.08	0.0601	4.54	1.99
6.58	0.509	2.72	1.98	24.32	0.116	6.67	2.93	27.72	0.0543	5.71	2.09
8.76	0.417	3.63	2.19	27.72	0.100	7.61	3.16	33.35	0.0432	6.86	2.34
10.69	0.341	4.43	2.42	30.38	0.088	8.34	3.37	38.45	0.0357	7.91	2.57
12.30	0.286	5.09	2.65	33.46	0.075	9.19	3.65	44.74	0.0286	9.20	2.88
13.64	0.266	5.65	2.74	37.21	0.060	10.21	4.09	53.54	0.0211	11.01	3.35
14.51	0.253	6.01	2.81	41.29	0.050	11.33	4.46	63.33	0.0183	13.02	3.60
15.12	0.230	6.26	2.95	44.53	0.040	12.22	5.00				
15.56	0.227	6.45	2.97	47.36	0.032	13.00	5.64				
16.01	0.217	6.63	3.03	49.91	0.026	13.70	6.21				
16.36	0.213	6.78	3.07	52.02	0.022	14.28	6.77				
16.61	0.185	6.88	3.29	54.68	0.017	15.01	7.79				
16.93	0.133	7.01	3.87								

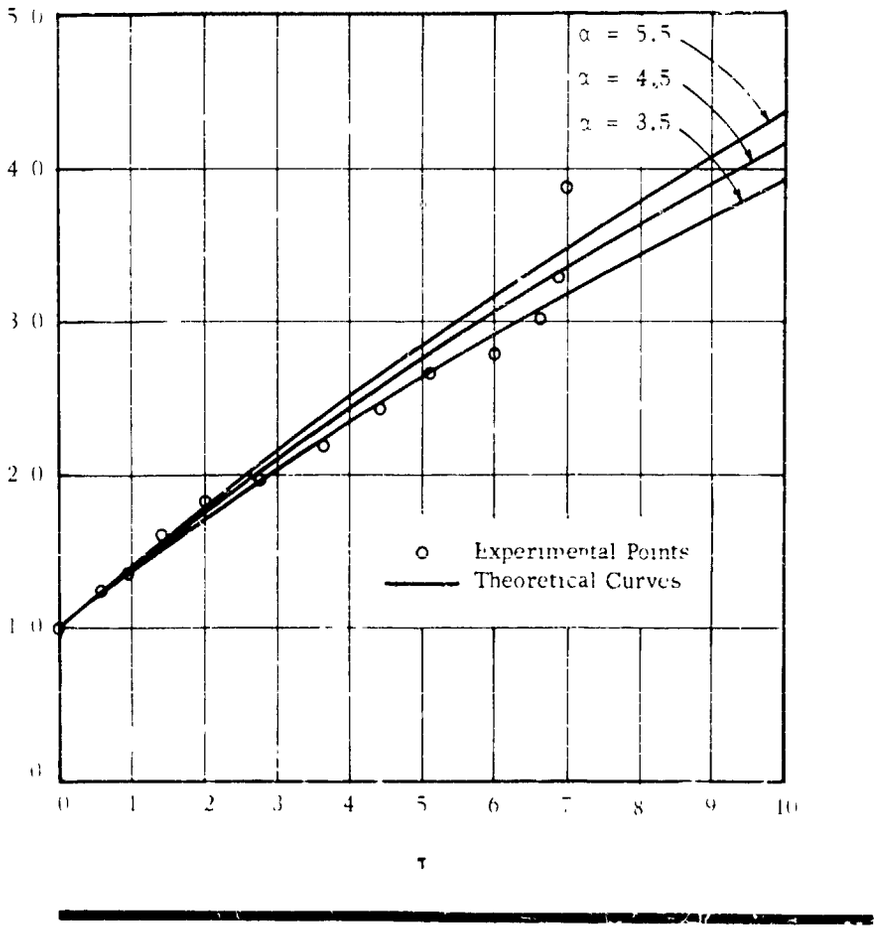

FIGURE 9 CORRELATION OF EXPERIMENTAL POINTS (SPHERE #2)

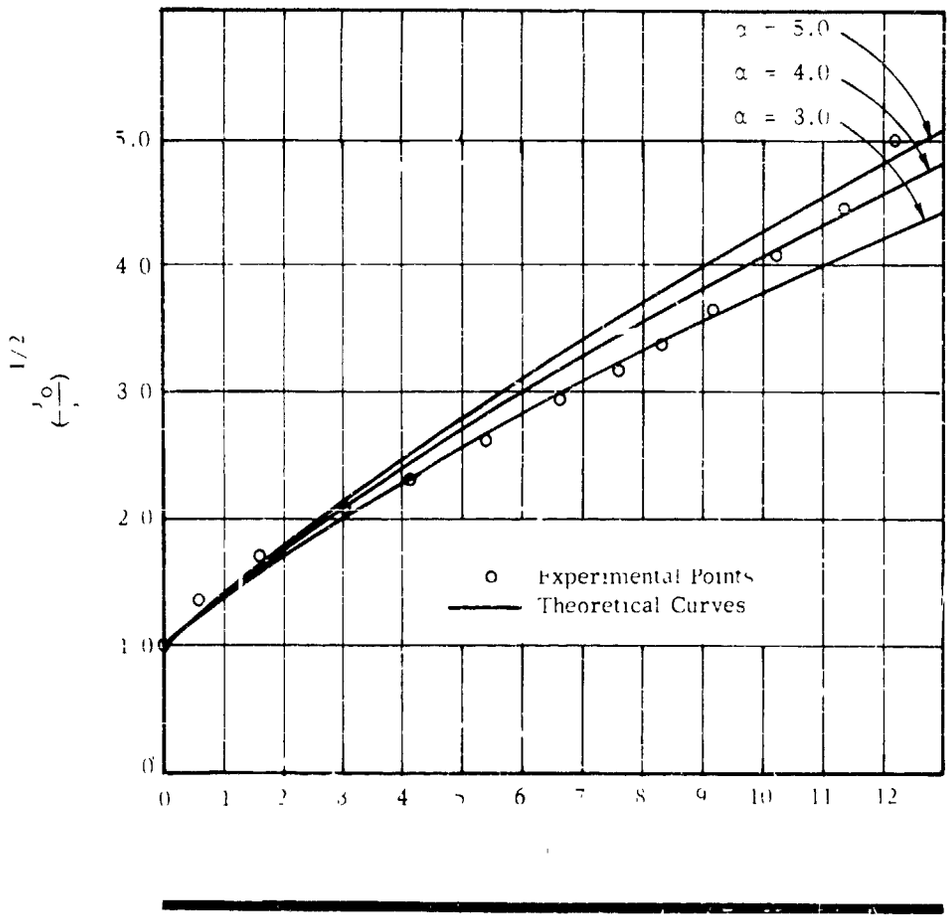

FIGURE 10 CORRELATION OF EXPERIMENTAL POINTS (SPHERE #3)

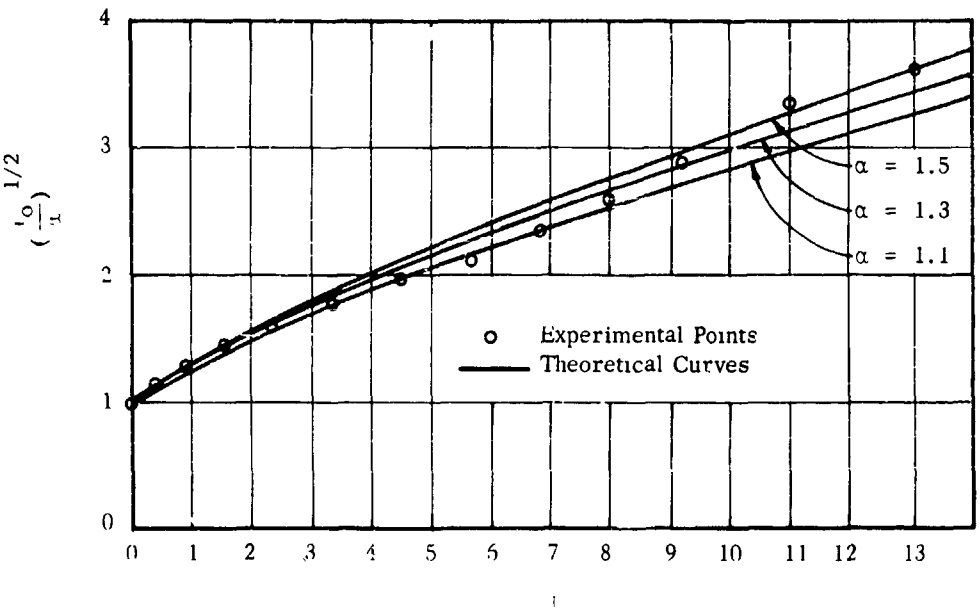

FIGURE 11 CORRELATION OF EXPERIMENTAL POINTS (SPHERE #5)

TABLE IV

EXPERIMENTAL DETERMINATION OF THE CONSTANT K

Sphere No.	Experimental Value of α	Computed Value of K
2	4.5	25
3	4.0	21
5	1.3	20
	Average Value of K:	22

VI. THE AERODYNAMIC PARAMETERS OF FULLY INFLATED BALLOONS

It is assumed that a fully inflated balloon at high altitudes can be idealized as a spherical shell.

For a balloon, the inside and outside gases are different (helium and air). The ratio of the value of $(\rho\mu)^{1/2}$ for helium to that for air is equal to about 0.40 and is independent of the altitude of the balloon. Applying the results of the preceding two sections, we obtain:

$$D = 2.5\,(\rho\mu)^{1/2}\,a^4\,\omega^{3/2} \tag{17}$$

$$I_A = 31\,(\rho\mu)^{1/2}\,a^4\,\omega^{-1/2} \tag{18}$$

where ρ and μ pertain to air and a is the equivalent radius of the balloon. Equations 17 and 18 are representations of Equations 7 and 16, respectively, for a helium filled sphere in air.

Equation 17 is valid for a steady rotation which satisfies the following two conditions:

1. The Reynold's number $(\rho\,\omega\,a^2/\mu)$ must be in the range 700 to 27,000.

2. The time of the duration of the steady rotation must be much less than $\rho\,a^2/\mu$. (For times much larger than $\rho\,a^2/\mu$, the contribution of the internal flow is negligible, and 2.5 in Equation 17 should be replaced by 1.6.)

The above two expressions are also applicable to an unsteady rotation which satisfies the following additional condition (see Section IV-B):

3. The angular acceleration must be small, i.e.:

$$\frac{d\omega}{dt} << \omega^2 \tag{19}$$

Consider a balloon with a radius of about 80 feet near ceiling at an altitude of 80 000 feet. At this altitude, the values of the

kinematic viscosity (μ/ρ) for the atmosphere and the helium inside the balloon are about 3.4×10^{-3} and 2.4×10^{-2} ft^2/sec, respectively. Therefore, condition 2 states that the duration of a steady rotation should be much smaller than 70 hours, which is easily satisfied in practice. Condition 1 requires that the angular velocity should not exceed 0.9 rad/sec, which is also satisfied in practice. As for condition 3, it is satisfied by the rather smooth oscillations of the November 1959 Project Strato-Lab Flight but not by the violent oscillations of earlier (1955 and 1935) balloon flights (see Figs. 2, 3, and 4 of Ref. 1).

Table V shows the values of D and I_A for two values of ω, representing roughly the maximum and minimum angular velocity of the above Strato-Lab Flight at ceiling. The radius of the balloon was about 80 feet. The weight of the balloon fabric, constructed of 2 mil polyethylene, was 1100 lbs. Therefore, the moment of inertia of the material of the balloon was about 1.5×10^5 slugs ft^2.

TABLE V

VALUES OF THE AERODYNAMIC EFFECTS FOR A BALLOON OF 80 FEET IN RADIUS AT AN ALTITUDE OF 80,000 FEET

Angular Velocity ω (rad/min)	Damping Aerodynamic Torque-D (ft lbs)	Apparent Additional Moment of Inertia I_A (slugs ft^2)
0.2	0.09	10^5
0.04	0.008	2.3×10^5

Thus, the apparent additional moment of inertia is comparable to that of the fabric in the range of angular velocities indicated in Table V. Considering the large size of the balloon, the total moment of inertia and the damping torque (aerodynamic) are, indeed, small. Small moment of inertia makes it easy to set the balloon in rotation, and small damping results in a very slow decay of the rotation. Hence, balloons can be very easily rotated.

Finally, we like to present a very brief review of the existing literature on the aerodynamic parameters of a rotating sphere and discuss their applicability to balloon rotations. Lamb (Ref. 6) has dealt with the problem of a sphere with sinusoidal rotation in a viscous fluid. Since balloons experience oscillating rotations frequently, it

appears, at first, that Lamb's results can be very useful in analyzing these rotations. However, he considered very small Reynold's numbers, in which case the convection terms in the momentum equation of the fluid can be neglected. Thus, he was able to solve in closed form this simplified linear problem (the general problem, with the convection terms included, is nonlinear). His results for the damping aerodynamic torque and apparent additional moment of inertia depend linearly on the amplitude of oscillation. Notice that, in Equations 12 and 18, the dependence of D and I_A on ω is nonlinear, which shows that the convection terms are included in our treatment. The Reynold's numbers involved in balloon rotations are high, and Lamb's results are not applicable.

Carrier and Di Prima (Ref. 7) considered the same problem with the convection terms. They formulated the solution in the form of an infinite series in ascending powers of the amplitude of oscillation, and they computed the first linear term (a special case of Lamb's solution) and the next quadratic term. Their two-terms solution is accurate enough when the following two conditions are satisfied. The first is a condition on the frequency of oscillation which can be satisfied only by the most rapid balloon oscillations. The second is, naturally, a restriction on the amplitude of oscillation (it must be small) which is not always satisfied by balloons. Carrier and Di Prima's results are so restrictive that they can be applied to the rotational oscillations of balloons only in special circumstances.

VII. DYNAMICS OF BALLOON ROTATIONS

Now, that the aerodynamic parameters of the balloon have been determined, the equations of motion may be written for the coupled rotations of the balloon-gondola system.

Let θ_1 and θ_2 denote the angular displacements of the balloon and gondola, respectively. Then the apparent additional moment of inertia (I_A) and the damping aerodynamic torque (D) of the balloon are given by (see Equations 17 and 18):

$$I_A = \alpha \left| \dot{\theta}_1 \right|^{-1/2} \tag{20}$$

$$D = \beta \dot{\theta}_1 \left| \dot{\theta}_1 \right|^{1/2} \tag{21}$$

A "dot" is used to denote the derivative with respect to time. The vertical bars mean "absolute value of". They are necessary, since I_A must be positive and D must oppose the motion always. The constants α and β are given by:

$$\alpha = 31 \, (\rho\mu)^{1/2} \, a^4 \tag{22}$$

$$\beta = 2.5 \, (\rho\mu)^{1/2} \, a^4 \tag{23}$$

Let I_1 and I_2 denote the fabric moments of inertia of the balloon and gondola, respectively, and k the effective torsional spring constant of the suspension system between balloon and gondola. Let τ_1 and τ_2 be the torques applied to the balloon and gondola, respectively. The equations of motion of the system are:

$$I_1 \ddot{\theta}_1 + \alpha \frac{d}{dt} \left(\dot{\theta}_1 \left| \dot{\theta}_1 \right|^{-1/2} \right) + \beta \dot{\theta}_1 \left| \dot{\theta}_1 \right|^{1/2} + k \, (\theta_1 - \theta_2) = \tau_1 \tag{24}$$

$$I_2 \ddot{\theta}_2 + k \, (\theta_2 - \theta_1) = \tau_2 \tag{25}$$

Aerodynamic effects on the gondola have been neglected. For specified applied torques, the angular displacements of the balloon and gondola can be found from the above equations.

A. SINUSOIDAL ANALYSIS: THEORY

Suppose that sinusoidal torques (τ_1 and τ_2) of given amplitude, frequency, and relative phase are applied to the system. Ultimately, the system will reach a periodic steady state. Due to the nonlinearities of the system, the angular displacements (θ_1 and θ_2) will have an infinite spectrum of harmonics in addition to the fundamental. The spectra of θ_1 and θ_2 can be computed, but the procedure is much more tedious than that of the reverse problem, that is to say, for given sinusoidal θ_1 and θ_2, compute the spectra of the required τ_1 and τ_2. With regard to the fundamental components, the two problems will give approximately the same results.

Let θ_1 and θ_2 be specified as follows.

$$\theta_1 = A_1 \cos \omega t \tag{26}$$

$$\theta_2 = A_2 \cos \omega t + A'_2 \sin \omega t \tag{27}$$

where A_1, A_2 and A'_2 are constants. Then, it can be shown that:

$$\dot{\theta}_1 |\dot{\theta}_1|^{-1/2} = -(\omega A_1)^{1/2}(1.11 \sin \omega t + 0.159 \sin 3\omega t + \ldots.) \tag{28}$$

$$\dot{\theta}_1 |\dot{\theta}_1|^{1/2} = -(\omega A_1)^{3/2}(0.917 \sin \omega t - 0.102 \sin 3\omega t + \ldots.) \tag{29}$$

Substituting Equations 26 to 29 in Equations 24 and 25, we find that τ_2 has only the fundamental component (ω) while τ_1 has an infinite number of components (ω, 3ω, 5ω ...). Let the fundamental components of τ_1 and τ_2 be denoted by:

$$\tau_1 = T_1 \cos \omega t + T'_1 \sin \omega t \tag{30}$$

$$\tau_2 = T_2 \cos \omega t + T'_2 \sin \omega t \tag{31}$$

where T_1, T'_1, T_2, and T'_2 are four unknown constants. They are determined from the following four equations:

$$T_1 = (-\omega^2 I_1 + k) A_1 - 1.11 \alpha \omega^{3/2} A_1^{1/2} - k A_2 \qquad (32)$$

$$T'_1 = -0.917 \beta \omega^{3/2} A_1^{3/2} - k A'_2 \qquad (33)$$

$$T_2 = (-\omega^2 I_2 + k) A_2 - k A_1 \qquad (34)$$

$$T'_2 = (-\omega^2 I_2 + k) A'_2 \qquad (35)$$

Equations 32 to 35 relate the fundamental components of the applied torques and angular displacements. Of the seven quantities (A_1, A_2, A'_2, T_1, T'_1, T_2, and T'_2), three must be specified. The remaining four can then be computed. The apparent paradox, that we cannot specify all the torques (T_1, T'_1, T_2, and T'_2), is resolved when it is noted that the phase of θ_1 has already been specified.

As the harmonic components decrease very rapidly (see, for instance, Equations 28 and 29), a solution, which involves only the fundamental components, is adequate in this highly nonlinear problem. The error is about 10 percent.

B. SINUSOIDAL ANALYSIS: NUMERICAL EXAMPLE

As a numerical example, we will consider the November 1959 Project Strato-Lab Flight at ceiling. Reasonable values for the parameters of the system are as follows:

$\alpha = 5.8 \times 10^3$ ft lbs $\text{sec}^{3/2}$

$\beta = 4.8 \times 10^3$ ft lbs $\text{sec}^{3/2}$

$I_1 = 1.5 \times 10^5$ slugs ft^2

$I_2 = 1{,}100$ slugs ft^2

$k = 110$ ft lbs

The calculation of α, β and I_1 has been based on idealizing the balloon as a spherical shell 80 ft in radius and weighing 1100 lbs. The value of I_2 was obtained by idealizing the gondola as a solid circular disk 9 ft in diameter and weighing 3500 lbs. It was observed during the flight that the period of torsional oscillations of the gondola with respect to the balloon ($2\pi(I_2/k)^{1/2}$) was about 20 seconds. Hence, the above value of k is obtained.

Since $I_1 >> I_2$, the resonant period of the system is very close to $2\pi(I_2/k)^{1/2}$. The value of this period is 20 seconds, corresponding to a frequency of 0.31 rad/sec. At resonance, a very small torque applied to the balloon produces small oscillations for the balloon and very large oscillations for the gondola, while a very small torque applied to the gondola produces very large oscillations for the entire system, especially for the gondola. The flight data (Fig. 3, Ref. 1) show that such a period was not present at ceiling. The minimum period was about 10 minutes and the maximum about 40 minutes, corresponding to maximum and minimum frequencies of 0.01 and 0.0025 rad/sec. Within this range of frequencies, we will compute from Equations 32 to 35 the angular displacements for given applied torques.*

First, consider the case of the torque being applied to the balloon only. Then the angular displacement of the gondola is approximately equal to that of the balloon. Both are approximately 180 degrees out of phase with the applied torque. The amplitude of the angular displacements is shown in Table VI for various values of the amplitude and frequency of the applied torque.

TABLE VI

AMPLITUDE OF ANGULAR DISPLACEMENT IN RADIANS FOR VARIOUS VALUES OF AMPLITUDE (T) AND FREQUENCY (ω) OF APPLIED TORQUE

ω rad/sec \ T ft lbs	1	1.7	3	3.4	5.8	10	12	21	39
0.0025	0.5	1	2						
0.005				0.5	1	2			
0.01							0.5	1	2

*Because these equations are nonlinear in A_1, it is much easier to do this computation in reverse; i.e., assume values of the displacement of the balloon (A_1) and compute the required torques and the displacement of the gondola

We see that, as the frequency increases, higher torques are required in order to have the same displacement. This is so, because the above frequencies are smaller than the antiresonant frequency of the system, which is equal to about 0.707 times the resonant frequency; i.e., 0.22 rad/sec.

Next consider the case of the same torque being applied to the gondola. Then, the angular displacements of the balloon and gondola are approximately in phase. They are approximately 180 degrees out of phase with the applied torque. The amplitude of the displacement of the balloon is again given by Table VI, but the amplitude of the displacement of the gondola is now different (Table VII). We see that, as the frequency increases, the displacement of the gondola becomes smaller than that of the balloon. This is so, because, in addition to the above discussed antiresonant frequency of the entire system, in this case the gondola has another antiresonant frequency. Due to the nonlinearities of the system, the value of this frequency depends on the amplitude of the applied torque. However, it can be shown that it cannot be larger than $(k/I_1)^{1/2} = 0.027$ rad/sec. Obviously, for the larger frequencies of Table VII, the gondola is near this antiresonance.

TABLE VII

AMPLITUDE OF ANGULAR DISPLACEMENT IN RADIANS FOR VARIOUS VALUES OF AMPLITUDE (T) AND FREQUENCY (ω) OF APPLIED TORQUE

ω rad/sec \ T ft lbs	1	1.7	3	3.4	5.8	10	12	21	39
0.0025	0.5	1	2						
0.005				0.5	0.9	1.9			
0.01							0.4	0.8	1.6

The above angular displacements are of the same order as those shown by the flight data. We see that the required torques are rather small. It seems that they can arise easily from aerodynamic effects (the wake behind the slowly rising or falling balloon, etc.). The smaller of these torques could, also, be caused by the motion of matter in the gondola (telescope, operator, navigator, etc.).

For the above frequencies and amplitudes of the applied torques, the aerodynamic damping on the balloon is very small, but the apparent

additional moment of inertia of the balloon is comparable to its material moment of inertia.

The criteria for improving the stability of the gondola depend on the place of application of the torque. In general, the moment of inertia of the gondola will be, at most, of the same order as the moment of inertia of the balloon. Then, when the torque is applied to the balloon, the stability of the gondola is improved as $k/I_2 \to 0$. On the other hand, when the torque is applied to the gondola, the stability of the gondola is improved as $k/I_1 \to \infty$. In other words, for torques applied to the balloon, the gondola must be decoupled from it; while, for torques applied to the gondola, the gondola must be well coupled to the balloon. These two criteria cannot be satisfied simultaneously. A compromise must be made, which will depend on the nature of the torques applied to the balloon and gondola. Considerable damping will, also, improve the stability of the system, but as pointed out already, the damping in balloons (aerodynamic) is very small.

REFERENCES

1. Arthur D. Little, Inc., "Balloon Dynamics, Technical Report No. 1," Contract Nonr-3164(00), February 27, 1961.

2. Goldstein, S., Editor, MODERN DEVELOPMENTS IN FLUID DYNAMICS, Oxford, 1957.

3. Magarvey, R. H., and Blackford, B. L., "Wake Metamorphism Behind a Sphere," CANADIAN JOURNAL OF PHYSICS, Vol. 40, No. 8, 1962.

4. Magarvey, R. H., and Bishop, R. L., "Wakes in Liquid-Liquid Systems," THE PHYSICS OF FLUIDS, Vol. 4, No. 7, 1961.

5. Magarvey, R. H., and Bishop, R. L., "Transition Ranges for Three-Dimensional Wakes," CANADIAN JOURNAL OF PHYSICS, Vol. 39, No. 10, 1961.

6. Lamb, H., HYDRODYNAMICS, Dover, 1945.

7. Carrier, G. F., and DiPrima, R. C., "On the Torsional Oscillations of a Solid Sphere in a Viscous Fluid," JOURNAL OF APPLIED MECHANICS, Vol. 23, pp. 601-605, December 1956.

DISTRIBUTION LIST

A. GOVERNMENT DISTRIBUTION	No. of Copies
Defense Documentation Center Cameron Station Alexandria 14, Virginia	20
Chief of Naval Research Attn: Physics Branch (Code 421) Washington 25, D. C.	3
Commanding Officer Office of Naval Research Branch Office 495 Summer Street Boston 10, Massachusetts	1
Director Naval Research Laboratory Technical Information Officer Washington 25, D. C.	2
Commanding Officer Office of Naval Research Branch Office 346 Broadway New York 13, New York	1
Commanding Officer Office of Naval Research Branch Office 230 N. Michigan Avenue Chicago 1, Illinois	1
Commanding Officer Office of Naval Research Branch Office 1000 Geary Street San Francisco 9, California	1
Commanding Officer Office of Naval Research Branch Office 1030 East Green Street Pasadena 1, California	1
Commanding Officer Office of Naval Research London Branch Office Navy #100 Fleet Post Office New York, New York	1

Office of Naval Research Field Representative
Navy Balloon Projects
Physics Department
University of Minnesota
Minneapolis 14, Minnesota 2

Commanding Officer
Physics Division
U. S. Naval Ordnance Test Station
Inyokern
China Lake, California 1

Commanding General
Air Research and Development Command
Attn: Office of Scientific Research
Washington 25, D. C. 2

Commander
Air Force Cambridge Research Laboratories
Hanscom Field
Bedford, Massachusetts 3

B. CIVILIAN DISTRIBUTION

National Center for Atmospheric Research
Boulder, Colorado 3

Professor E. P. Ney
Physics Department
University of Minnesota
Minneapolis, Minnesota 1

Professor Martin Schwarzschild
The Observatory
Princeton University
Princeton, New Jersey 1

Dr. G. Newkirk
High Altitude Observatory
Boulder, Colorado 1

Mr. Arthur A. Anderson
Aerospace Research Department
General Mills, Inc.
St. Paul, Minnesota 1

Mr. Richard J. Slater G. T. Schje Dahl Company Northfield, Minnesota	1
Mr. James G. Nelson Minneapolis-Honeywell Regulator Company Minneapolis, Minnesota	1
Dr. John D. Strong Johns Hopkins University Baltimore, Maryland	1
Mr. Russell A. Nidey Kitt Peak National Observatory Tucson, Arizona	1
Dr. Alvin H. Howell College of Engineering Tufts University Medford, Massachusetts	1
Dr. J. Allen Hynek Dearborn Observatory Northwestern University Evanston, Illinois	1
Mr. Robert S. Ross Goodyear Aerospace Corporation Akron, Ohio	1
Mr. Arthur Dewey Struble, Jr. Sea-Space Systems, Inc. Torrance, California	1
Mr. James A. Menke Anoka Facility Viron Division Geophysics Corporation of America Anoka, Minnesota	1
Mr. James R. Smith Raven Industries, Inc. Sioux Falls, South Dakota	1
Mr. Robert M. Nelson Dewey and Almy Chemical Division W. R. Grace and Company Cambridge, Massachusetts	1